# Magnetic susceptibility of the hippocampal subfields and basal ganglia in acute mild traumatic brain injury

**Christi A. Essex[a,*], Mayan J. Bedggood[a], Jenna L. Merenstein[b], Catherine Morgan[c, d], Helen C. Murray[e], Samantha J. Holdsworth[f], Richard L. M. Faull[e], Patria Hume[g], Alice Theadom[a], Mangor Pedersen[a]**
[a]Department of Psychology and Neuroscience, Auckland University of Technology, Auckland 0627, New Zealand
[b]Brain Imaging and Analysis Center, Duke University Medical Center, Durham, NC 27710, United States
[c]Center for Advanced MRI, The University of Auckland, Auckland 1023, New Zealand
[d]School of Psychology and Centre for Brain Research, The University of Auckland, Auckland 1023, New Zealand
[e]Center for Brain Research, The University of Auckland, Auckland 1023, New Zealand
[f]Mātai Medical Research Institute, Gisborne 4010, New Zealand
[g]Sports Performance Research Institute New Zealand, Auckland University of Technology, Auckland 0627, New Zealand

*Christi A. Essex: christi.essex@autuni.ac.nz

**Abstract.** Despite vulnerability to microstructural tissue damage following mild traumatic brain injury (mTBI), key subcortical brain regions have been overlooked in quantitative susceptibility mapping (QSM) studies. Alterations to tissue composition in the functionally and structurally distinct hippocampal subfields and basal ganglia regions may reflect distinct symptomatology, and better characterisation of these regions is needed to increase our understanding of mTBI pathophysiology. To address this issue, we used magnetic source-separated QSM to quantify spatial distributions of positive (iron-related) and negative (myelin-, protein-, and calcium-related) magnetic susceptibility across 10 hippocampal substructures and 16 segmentations of the basal ganglia in 25 male participants with acute ($<$ 14 days) sports-related mTBI (sr-mTBI). Additional variables of interest including age, injury severity, and days since injury at time of the magnetic resonance imaging (MRI) scan were also correlated with both positive and negative susceptibility values. Primary analyses indicated no significant difference in positive susceptibility values between sr-mTBI participants and controls for hippocampal and basal ganglia ROIs. For negative sign values, susceptibility was significantly less negative for sr-mTBI participants in the cornu ammonis 4 (CA4) region only ($p$FDR $< 0.05$). In line with the known linear relationship between iron deposition and age in deep grey matter sites, particularly within the first three decades of life, significant positive relationships were observed between positive susceptibility and age in the putamen, caudate, red nucleus, parabrachial pigmented nucleus, and ventral pallidum ($p$FDR $< 0.05$). Positive relationships were also observed between absolute negative susceptibility values and age in the hippocampal fimbria, caudate, and extended amygdala ($p$FDR $< 0.05$), suggesting age-related calcifications in these regions. A negative relationship was observed between negative absolute values and age in the ventral pallidum ($p$FDR $< 0.05$), indicating potential changes to myelin content in this region. No significant associations were observed between any other variable and signed susceptibility values. The results of this study contribute to, and extend, prior literature regarding the temporal kinetics of biomagnetic substrates as a function of ageing. Decreased negative susceptibility after mTBI in the CA4 region also suggests potential injury-related effects on myelin content or cell loss; a particularly interesting finding in light of the well-established vulnerability of this region to pathology in chronic traumatic encephalopathy (CTE). The lack of other significant between-group differences suggest that alterations to tissue content may not be quantifiable at the acute stage of injury in subcortical ROIs or may be masked by age-related tissue susceptibility changes as a common feature across all participants in this young cohort. Future research should consider the use of longitudinal study designs to mitigate the potential influence of these factors.

**Keywords:** basal ganglia; brain iron; concussion; hippocampal subfields; mild traumatic brain injury; quantitative susceptibility mapping.

## Introduction

Whilst participation in sports can have many physical and psychological benefits, there is a non-negligible risk of sustaining a mild traumatic brain injury (mTBI). This is the most common form of TBI,[1] and reports suggest that up to 30% of all TBI cases are mild head injuries resulting from sports participation.[2] The related changes to cognition, mental health, and physiology can be far from what categorisation as a "mild" injury would suggest, significantly degrading quality of life and participation in activities of daily living.[3] These symptoms are generally associated with the acute and subacute stages, but may persist for decades after injury.[4–6] In addition, repeated instances of mild head trauma expose individuals to a mTBI-related form of progressive neurodegeneration, chronic traumatic encephalopathy (CTE),[3,7] and increased risk of premature mortality.[8] Given the popularity of sports the world over, the issue of mTBI warrants careful consideration.

A mTBI is induced by either impact or inertial forces[9] which transmit mechanical energy to the brain[10] causing primary and secondary injury.[11] Primary injury occurs at the time of the incident when the brain is displaced within the skull, damaging the neurons, glia, and blood vessels of the cerebral tissues.[12] mTBI is most often associated with a diffuse primary injury, specifically diffuse axonal injury, whereby the cellular nerve

fibers are stretched, causing cytoskeletal damage.[11,13,14] Secondary injury refers to the resultant dynamic physiological processes catalysed by the primary injury; this complex and self-perpetuating cascade of biomechanical and metabolic disturbance within the affected tissues can propagate for months after the initial impact.[15] This includes, but is by no means limited to, altered neurotransmitter signalling, changes to cerebral blood flow, mitochondrial dysfunction, blood-brain barrier (BBB) disruption, oxidative stress, demyelination, and neuroinflammatory responses.[9,11,16] However, the underlying pathophysiology of mTBI remains poorly understood.[14]

Iron is an essential co-factor for many neuronal processes including mitochondrial respiration, oxygen transport, cellular metabolism, and synthesis of neurotransmitters, myelin, and DNA.[17,18] However, iron overload, particularly in non-heme form (i.e., iron bound to proteins like ferritin and transferrin rather than heme groups), is increasingly recognised as a driver of secondary neurotoxic events[11,19] including oxidative stress, cellular degeneration, and inflammation.[20–22] Non-heme iron is also the primary source of paramagnetic signals assessed by quantitative susceptibility mapping (QSM), an analytical technique of magnetic resonance imaging (MRI) data that enables quantification of biomagnetic substances in neural tissue.[23–26] As such, mapping distributions of positive susceptibility across the brain as a proxy for iron load represents a promising avenue for investigating potential biomarkers of neuropathology following mTBI. Myelin constitutes the primary source of diamagnetic contrast on QSM,[27] but calcium[28–30] and certain proteins such as beta-amyloid (A$\beta$) and tau also contribute[31–33] and concentrations of all aforementioned biomagnetic substrates may change as a function of injury-related processes in mTBI.[11,16,22,34] Threshold-based isolation of these susceptibility sources may therefore provide crucial insight into the subtle biodynamics and injury cascades occurring shortly after injury. This type of approach to date has been overlooked in QSM investigations of mTBI.

In addition, research using QSM to examine alterations to grey matter after mTBI have focused on markers of iron accumulation in the basal ganglia as a proxy for secondary injury processes. Iron, as a fundamental component of neurotransmitter synthesis, is more abundant in these deep regions compared to cortical grey matter[35] to support the high metabolic demand related to signal processing and output.[11] Elevated concentration of iron is particularly noteworthy in the globus pallidus, red nucleus, substantia nigra, putamen, caudate, and thalamus[35] and may predispose these regions to iron-mediated disorders.[36] Additional vulnerability to shear and strain damage in mTBI[37] due to axons originating from, terminating in, or intersecting with these nuclei,[11,38,39] for example thalamo-cortical projections,[40] may exacerbate the risk of iron-driven secondary injury.

Within this existing body of research, a focus on either total deep grey matter,[41,42] basal ganglia segmentations,[43–45] or a combination of both approaches,[46,47] has predominated. Where segmentations are used, primarily only major subcortical structures such as the caudate, putamen, thalamus, and intact globus pallidus[43,44,46] have been investigated, overlooking the susceptibility of many other regions to cytotrauma. To date, only two studies[45,47] have extended their investigations to include additional subcortical structures such as the nucleus accumbens, amygdala, and hippocampus, which exhibit similar iron-related vulnerability as the basal nuclei. However, even these more comprehensive investigations fall short with regard to differentiation of the hippocampal subfields and other deep nuclei of potential interest, representing a crucial oversight in the QSM-mTBI literature.[11] These include distinct pallidal substructures (comprising the globus pallidus internus and externus, and the ventral pallidum), the substantia nigra (pars reticulata and pars compacta), and limbic structures such as the extended amygdala, hypothalamus, and mammillary nucleus, the mesolimbic ventral tegmental area and associated subregions (i.e., parabrachial pigmented nucleus, epithalamic habenular nuclei, and subthalamic nucleus) and the red nucleus. Examining these additional subregions may be critical for identifying potentially more subtle mTBI-related changes to biomagnetic substrates that could otherwise be washed out when examining entire regions-of-interest (ROI), as we have previously demonstrated in the cortical grey matter.[48]

Pathology in these deep brain structures responsible for motor control and movement,[49] emotional regulation,[50] learning,[51] and memory,[52] may contribute to differences in mTBI symptom presentation, severity, and injury burden between participants. Iron overload in the deep grey matter in particular may significantly alter cognitive function after mTBI.[53] As such, the subcortical nuclei warrant careful and thorough investigation. In addition, examining the hippocampus using a whole-ROI approach neglects the structural and functional distinctions between its subfields. The hippocampus is particularly vulnerable to injury,[54] and as a central hub for memory[55] damage to this area may be related to the memory impairments characteristic of mTBI.[56] Macroscopic methods may thus risk masking specific hippocampal pathologies that are likely related to acute and chronic mTBI symptomatology. One thing to note is that the temporal regions including the hippocampus are regions of focal atrophy and hyperphosphorylation of tau (p-tau) in CTE,[57,58] which may also be related to iron dyshomeostasis.[59]

Taken together, these studies suggest that investigations differentiating between distinct brain regions and their substructures are necessary to better understand the pathology of mTBI, and may assist in elucidating the genesis of specific injury-related deficits. To contribute to the sparse extant literature, we conducted the first QSM analysis of mTBI effects in the hippocampal subfields alongside the most detailed segmentation of the basal ganglia to date. This study aimed to: 1) assess the effects of mTBI on positive (iron-related) and negative (myelin-, protein-, calcium-related) magnetic susceptibility to better understand acute pathology in, a) 16 segmentations of the basal ganglia, and b) 10 segmentations of the hippocampus; and 2) elucidate the relationship between magnetic susceptibility in these regions and potentially moderating variables including age, and injury latency and severity. Although many of these regions are both high in iron and susceptible to mTBI-related pathology, the limited prior literature has produced mixed results regarding the direction of iron-related effects, if any. Furthermore, the absence of source separation in previous studies precludes the development of robust hypotheses regarding potential observations related to the directionality of diamagnetic effects and the underlying neurobiological properties. As such, there were no specific *a priori* hypotheses related to either susceptibility sign, nor secondary correlational analyses.

## Materials and Methods

Ethical approval for this research was obtained from the Health and Disabilities Ethics Committee (HDEC) (Date: 18/02/2022, Reference: 2022 EXP 11078) and institutional approval was also obtained from the Auckland University of Technology Ethics Committee (AUTEC) (Date: 18/02/2022, Reference: 22/12). In accordance with the Declaration of Helsinki, all participants provided written informed consent prior to data collection.

### *Participants*

Data from 25 male contact sports players ($M$ = 21.10 years old [16-32], $SD$ = 4.59) with acute sports-related mTBI (sr-mTBI) ($<$ 14 days; $M$ = 10.40 days, $SD$ = 3.03) and 25 age-matched male controls ($M$ = 21.10 years old [16-32], $SD$ = 4.35) were used for this observational study (see Table 1). To mitigate any potential confounding effects due to the known linear relationship between brain iron content and age, particularly in youthful cohorts, we ensured that ages were not significantly different between groups ($t(48) = 0.00$, $p = 1.00$). Clinical sr-mTBI participants were recruited through three Axis Sports Medicine clinics (Auckland, New Zealand), via print and social media advertisements, word-of-mouth, and through community-based pathways including referrals from healthcare professionals and sports team management. Each clinical participant was required to have a confirmed sr-mTBI diagnosis by a licensed physician as a prerequisite for study inclusion, and symptom severity was assessed using the Brain Injury Screening Tool (BIST)[60] either upon presentation to Axis clinics or electronically following recruitment. Healthy controls (HC) were recruited through print and social media advertisements, and word-of-mouth. Exclusion criteria for all participants included a history

of significant medical or neurological conditions unrelated to the study's objectives and contraindications for MRI. Additionally, controls were excluded if they had any recent history of mTBI events ($<$ 12 months) or were living with any long-term effects of previous mTBI. All participants completed a brief demographic questionnaire and attended a 1-hour MRI scan at The Centre for Advanced MRI (CAMRI), Auckland, New Zealand. All scans were reviewed by a certified neuroradiologist consultant for clinically significant findings. While some incidental findings were identified, none were considered to be clinically significant nor required follow-up. MRI findings for this cohort are reported in extensive detail in previous publications.[48]

Table 1: Summary of sr-mTBI participant clinical characteristics

| **ID** | **Age** | **DSI** | **BIST Score** | **MOI** |
|---|---|---|---|---|
| mTBI-01 | $<$ 20 | 5 days | 140 | Rugby |
| mTBI-02 | $<$ 20 | 5 days | 12 | Rugby |
| mTBI-03 | 20s | 6 days | 78 | Rugby |
| mTBI-04 | $<$ 20 | 13 days | 18 | Rugby |
| mTBI-05 | $<$ 20 | 12 days | 61 | Rugby |
| mTBI-06 | 20s | 13 days | 42 | Rugby |
| mTBI-07 | 20s | 13 days | 13 | Football |
| mTBI-08 | 20s | 12 days | 6 | Hockey |
| mTBI-09 | 20s | 6 days | 56 | Rugby |
| mTBI-10 | $<$ 20 | 12 days | 54 | Rugby |
| mTBI-11 | 20s | 10 days | 52 | Rugby |
| mTBI-12 | 30s | 13 days | 13 | Football |
| mTBI-13 | $<$ 20 | 5 days | 79 | Rugby |
| mTBI-14 | 20s | 13 days | 2 | Rugby |
| mTBI-15 | $<$ 20 | 13 days | 22 | Rugby |
| mTBI-16 | $<$ 20 | 8 days | 117 | Futsal |
| mTBI-17 | 20s | 13 days | * | Rugby |
| mTBI-18 | 20s | 10 days | 34 | Gymnastics |
| mTBI-19 | 20s | 13 days | 28 | Jiu-jitsu |
| mTBI-20 | 20s | 11 days | 69 | Surfing |
| mTBI-21 | $<$ 20 | 7 days | 14 | Rugby |
| mTBI-22 | $<$ 20 | 13 days | 39 | Judo |
| mTBI-23 | $<$ 20 | 9 days | 34 | Rugby |
| mTBI-24 | $<$ 20 | 12 days | 68 | Rugby |
| mTBI-25 | 20s | 12 days | 17 | Rugby |
| **Mean** | 21.10 (4.59) years | 10.4 (3.03) days | 44.5 (35.0) /160 | |
| **Mean HC** | 21.10 (4.35) years | | | |

*Note.* Diagnostic assessment was limited to the volume T1, SWI and DWI sequences with only limited interpretation of the multi-echo T2 stack. Clinical assessments were relevant to the identification of micro-haemorrhages, areas of siderosis, T1 appearance, gliosis, volume, ventricular volumes and non-neurological findings. Age is reported in a range to prevent re-identification of participants. The possible range of BIST scores is 0 (min) to 160 (max). Clinical group data corresponded to date at MRI only with the exception of the BIST[60] acquired $>$24 hours post-injury prior to MRI scanning ($<$14 days post). Abbreviations are: ID = unique identifier; DSI = days since injury; BIST = Brain Injury Screening Tool[60]; MOI = mechanism of injury; MRI = magnetic resonance imaging; L = Left; R = right; * = missing data (BIST incomplete on the Axis Sport Medicine Clinic patient portal, reason unknown).

*Neuroimaging*

Details on image acquisition and processing have been previously reported,[48] and are summarised here for brevity.

### *Acquisition*

MRI data were acquired on a 3T Siemens MAGNETOM Vida Fit scanner (Siemens Healthcare, Erlangen, Germany) equipped with a 20-channel head coil. A 3D flow-compensated GRE sequence was used to obtain magnitude and unfiltered phase images suitable for QSM reconstruction. Data were collected at 1 mm isotropic voxel size with matrix size = 180 x 224 x 160 mm, TR = 30 ms; TE = 20 ms; FA = 15°; FoV = 224 mm in a total acquisition time of ∼3.43 minutes. For each participant, a high-resolution 3D T1-weighted (T1w) anatomical image volume was acquired for coregistration, parcellation and segmentation using a Magnetisation-Prepared Rapid Acquisition Gradient Echo (MPRAGE) sequence (TR = 1940.0 ms; TE = 2.49 ms, FA = 9°; slice thickness = 0.9 mm; FoV = 230 mm; matrix size = 192 x 512 x 512 mm; GRAPPA = 2; voxel size 0.45 x 0.45 x 0.90 mm) for a total acquisition time of ∼4.31 minutes. DICOMs were converted to NIfTI files and transformed to brain imaging data structure (BIDS)[61] for further processing using *Dcm2Bids*[62] version 3.1.1, which is a wrapper for *dcm2niix*[63] (v1.0.20230411).

### *QSM processing*

QSM images were reconstructed using QSMxT[64] v6.4.2 (see QSMxT GitHub) and used a robust two-pass combination method for artefact reduction.[65] QSM images were reconstructed using a rapid open-source minimum spanning tree algorithm (ROMEO),[66] background field removal with projection onto dipole fields (PDF),[67] and sparsity-based rapid two-step dipole inversion (RTS)[68]; a pipeline congruent with recent consensus statement recommendations for best-practice QSM reconstruction.[69]

For each participant, the raw magnitude image was skull-stripped using FSL's *BET*[70] with robust brain centre estimation and a fractional intensity threshold of between 0.3 and 0.6. Binary masks were derived from the skull-stripped magnitude image and applied to the susceptibility maps to erode non-brain signal around the brain perimeter using *fslmaths*. Skull-stripped magnitude images were linearly coregistered to the California Institute of Technology's 168 (CIT168) T1w standard brain atlas[71] in the Montreal Neurological Institute's 152 brain atlas (MNI152) space using FMRIB's Linear Transformation Tool (FLIRT)[72–74] with 12 degrees of freedom (DoF) suitable for atlas-based registration. The resulting transformation matrix was then used for spatial normalisation of the QSM images using FLIRT.[72–74] Using inter-voxel thresholding methods,[75] QSM maps were then thresholded into separate maps of predominantly paramagnetic ($QSM^+$) from predominantly diamagnetic ($QSM^-$) voxels with *fslmaths*, by separating values across voxel boundaries above ($QSM^+$) and below ($QSM^-$) zero. Traditional QSM maps represent an aggregate of the susceptibility within voxels,[76] and this intra-voxel averaging may obscure individual susceptibility sources within a voxel. Further confounding effects can be introduced when averaging across voxels during analysis. The thresholding approach described here may help to address the latter limitation by isolating predominantly paramagnetic (iron-related) voxels from diamagnetic (myelin-, calcium-, and protein-related)[23,28–33] voxels, enabling more targeted analyses of specific susceptibility sources without the confounding effects of of inter-voxel averaging. Both $QSM^+$ and $QSM^-$ susceptibility maps were used in subsequent analyses.

### *Basal ganglia segmentation*

The CIT168 basal ganglia mask, available in MNI152 standard space, offers a detailed 16-part bilateral segmentation of the basal nuclei[71] and is openly accessible through the NeuroVault Collection (No. 3145). The segmentations included: the striatum, comprised of the putamen (Pu),

caudate (Ca), and nucleus accumbens (NAC); the pallidum, which includes the globus pallidus externus (GPe), globus pallidus internus (GPi), and ventral pallidum (VeP); and the substantia nigra, including the substantia nigra pars compacta (SNc) and substantia nigra pars reticulata (SNr). Additional segmentations covered the extended amygdala (EXA) and other limbic structures including the hypothalamus (HTH) and mammillary nucleus (MN), the mesolimbic ventral tegmental area (VTA) and the associated parabrachial pigmented nucleus (PBP), the epithalamic habenular nuclei (HN), the subthalamic nucleus (STH), and the red nucleus (RN) (see Fig. 1 for reference).

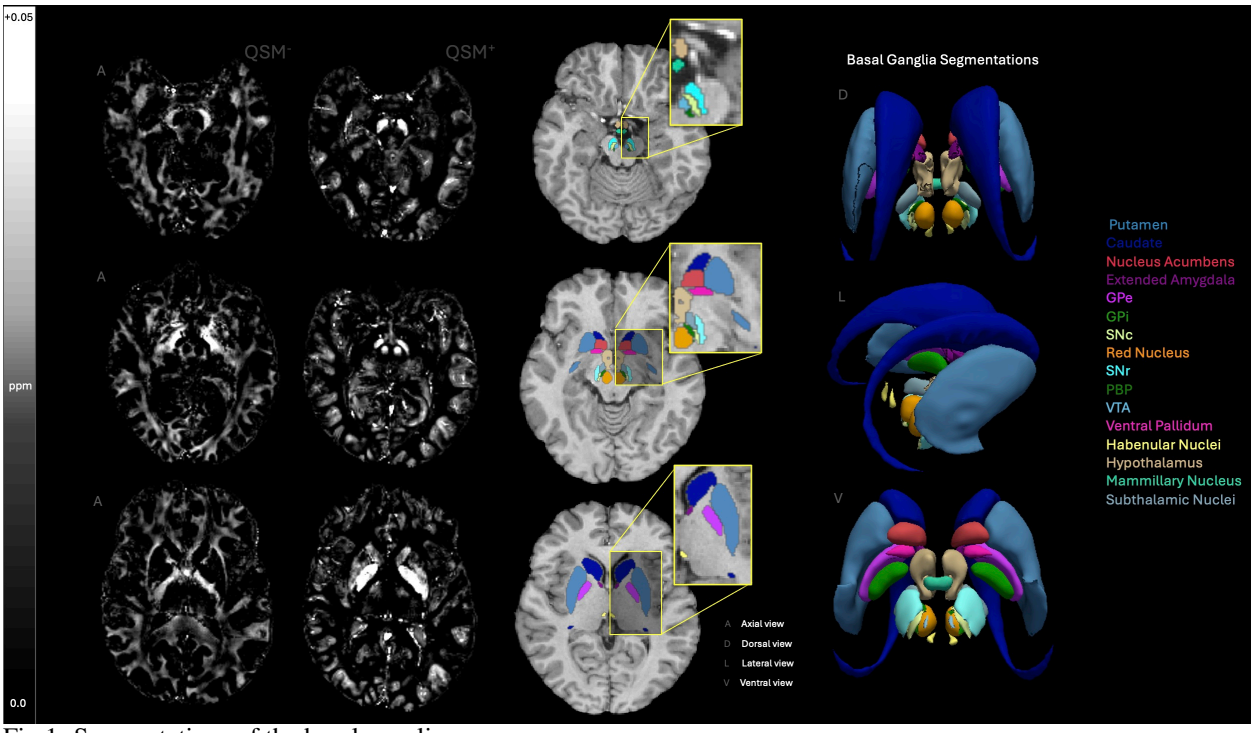


Fig 1: Segmentations of the basal ganglia

Sixteen bilateral segmentations of the basal ganglia are displayed across axial (A) slices of the T1w CIT168-MNI152 brain template, as well as 3D renderings from ventral (V), dorsal (D), and lateral (L) perspectives for both the CIT168-MNI152 brain template and corresponding basal ganglia mask. The key for each basal nuclei is provided in the respective colour of that region. Axial slices for signed maps ($QSM^-$ and $QSM^+$) are shown at comparable depths for visual reference. Susceptibility values are expressed in parts per million (ppm) ranging from 0.0 to +0.05, and negative maps are multiplied by -1 for better visualisation. GPe = globus pallidus externus; GPi = globus pallidus internus; SNc = substantia nigra pars compacta; SNr = substantia nigra pars reticulata; PBP = parabrachial pigmented nucleus; VTA = ventral tegmental area.

### *Hippocampal segmentation*

Prior to hippocampal segmentation, bias field correction was applied to each participants' T1w images using the *N4* algorithm[77] from ANTs.[78] The bias field-corrected T1w images were then processed with FreeSurfer's *recon-all* pipeline.[79] Subsequent unilateral segmentation of the hippocampal subfields was conducted using an automated, FreeSurfer-based pipeline.[80] This hippocampal segmentation leverages a probabilistic atlas derived from ultra-high-field, *ex vivo* MRI data with approximately 0.1 mm isotropic voxel resolution to automate the delineation of hippocampal substructures for each hemisphere. Three resulting hippocampal segmentation schemes were produced, a macroscopic head/body/tail segmentation (denoted as "HBT"), a detailed scheme where molecular subregions are merged with the nearest neighbours, specifically the CA subfields (labeled "CA"), and a detailed segmentation where molecular subregions are not merged (referred to as "FS60"). Of these, the mid-detail segmentation (the "CA" scheme) was selected for use in statistical analysis, balancing the level of segmentation detail with the need to mitigate the multiple comparisons

problem. The hippocampal subregion masks included in this segmentation: the parasubiculum, presubiculum, subiculum, cornu ammonis (CA) regions CA1, CA3 (which includes CA2), and CA4, the hippocampal-amygdala transition area (HATA), fimbria, hippocampal tail, and hippocampal fissure (see FreeSurfer Documentation). For full segmentation details, refer to Table 2, and for visual representation see Fig. 2.

Table 2: Hippocampal subfields and their closest anatomical structures in "CA" segmentation

| | |
|---|---|
| Parasubiculum | Parasubiculum |
| Presubiculum head | Presubiculum |
| Presubiculum body | |
| Subiculum head | Subiculum |
| Subiculum body | |
| CA1 head | CA1 |
| CA1 body | |
| CA3 head | CA3 |
| CA3 body | |
| CA4 head | CA4 |
| CA4 body | |
| GC-ML-DG head | |
| GC-ML-DG body | |
| Molecular layer HP-head | Closest structure* |
| Molecular layer HP-body | |
| HATA | HATA |
| Fimbria | Fimbria |
| Hippocampal tail | Hippocampal tail |
| hippocampal fissure | hippocampal fissure |

* = voxels in the molecular layer are assigned the label of the closest voxel that is neither molecular layer nor background. *Note.* This table details the unilateral segmentations of hippocampal subfields within the volume labelled as "CA", along with associated hippocampal structures. Subfield CA2 is incorporated into CA3. Table replicated from FreeSurfer Documentation.

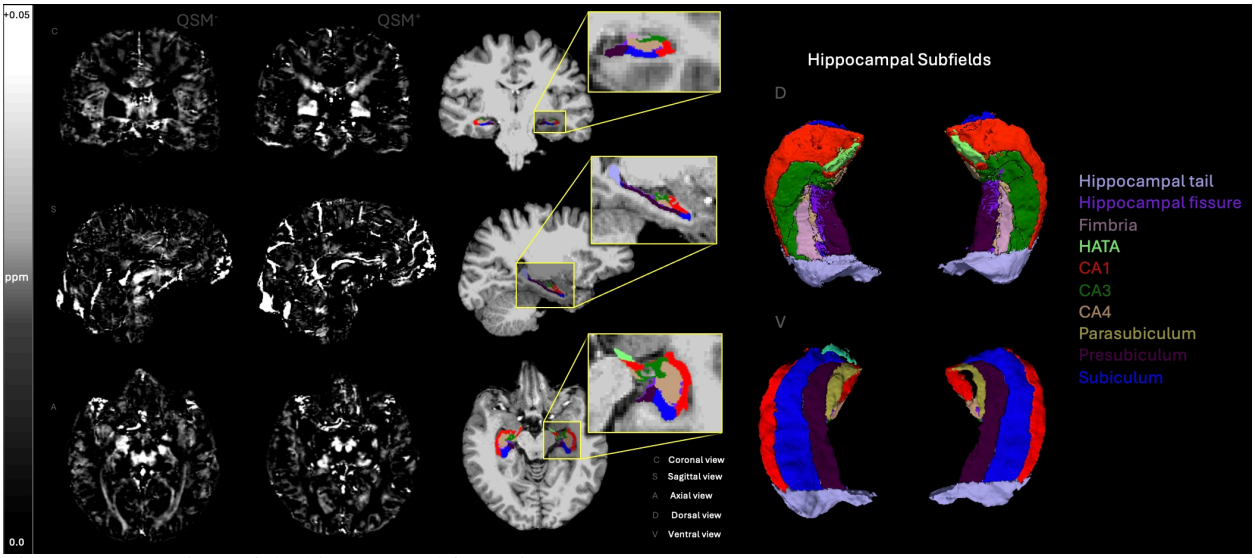


Fig 2: Segmentations of the hippocampal formation

Visual representation of the unilateral hippocampal segmentations provided by FreeSurfer under the "CA" scheme, displayed across coronal (C), axial (A), and sagittal (S) views as well as a 3D rendering from the ventral (V) and dorsal (D) views. The key for each hippocampal region is provided in the respective colour of that region. Signed maps ($QSM^-$ and $QSM^+$) from which susceptibility values are sampled for each hippocampal region are shown for each orientation (C, A, S). Susceptibility values are expressed in ppm ranging from 0.0 to +0.05, and negative maps are multiplied by -1 for better visualisation. HATA = hippocampal-amygdala transition area; CA 1-4 = cornu ammonis regions 1-4; note: CA2 is included in CA3.

To standardise each of the hippocampal subfield masks for data analysis, each subjects' skull-stripped T1w brain image and left and right hemisphere hippocampal masks were converted from FreeSurfer's .mgz format to NIfTI format (.nii.gz) using MRtrix3 *mrconvert*.[81] After format conversion, each subjects' T1w brain image was coregistered to the CIT168 T1w standard brain atlas in MNI152 space[71] using FLIRT[72–74] with 12 DoF. The resulting transformation matrix was then applied to both the left and right hemisphere hippocampal masks using nearest-neighbour interpolation to maintain the integrity of discrete hippocampal label boundaries during transformation. These steps ensured spatial alignment between each of the hippocampal masks, the signed susceptibility maps, and the CIT168 segmentations of the basal ganglia provided in MNI152 space.[71]

**Statistical analyses**

Statistical analyses were conducted at the bilateral level using MATLAB (2024a). Average positive and negative susceptibility values from both $QSM^+$ and $QSM^-$ maps were extracted from the 16 bilateral segmentations of the basal ganglia. For the 10 hippocampal regions, left and right hemisphere susceptibility values were extracted and averaged to yield a bilateral measure. Any ROIs in which zero values were present for any participant were omitted from subsequent analysis (the PBP for $QSM^-$ analyses, and the HN for $QSM^+$ analyses). There were no zero values for any participants for any hippocampal ROIs. To evaluate the effects of sr-mTBI compared to healthy controls, two-tailed independent sample t-tests were performed for each subcortical ROI, assessing group differences in susceptibility values. To control for multiple comparisons, a Benjamini-Hochberg false discovery rate (FDR) correction[82] was applied separately to the 15 p-values corresponding to the remaining basal nuclei (all nuclei except the PBP for $QSM^-$ and HN for $QSM^+$) and the 10 p-values for the hippocampal regions, for each signed susceptibility map. Since participants were precisely age-matched, age was not treated as a covariate or confounding factor in the between-group comparisons. However, to examine the associations between QSM values and age across the entire cohort, partial Pearson correlation coefficients were computed. These analyses assessed the potential linear relationship between age and both positive and negative susceptibility values across all subcortical ROIs, controlling for group status. Additional relationships were explored between susceptibility values and sr-mTBI-related variables using Pearson correlation coefficients, including BIST[60] scores and injury latency (days since injury; DSI) variables, for clinical participants only. Due to missing BIST[60] data, mTBI-17 was excluded from analyses related to injury severity. Correlations were also corrected for 15 and 10 ROI-wise comparisons, respectively, using FDR procedures.[82]

**Results**

*Regional analyses*

Using two-tailed independent sample t-tests, differences in bilateral regional susceptibility (positive and negative) were examined for each of the hippocampal subfields and basal nuclei. P-values were corrected for 10 and 15 comparisons, respectively, using FDR procedures.[82]

*Basal nuclei*

Results showed no significant differences in positive or negative susceptibility between sr-mTBI participants and HC for any of the basal nuclei ($p$FDR $> 0.05$; see Fig. 3).

*Hippocampal subfields*

There were no significant differences in positive susceptibility between groups for any of the 10 hippocampal subfields ($p$FDR $> 0.05$; see Fig. 3). Negative susceptibility values were significantly less negative for sr-mTBI participants ($M$ = -0.007, $SD$ = 0.002) than HC ($M$ = -0.008, $SD$ = 0.001) in the CA4 only ($t(48)$ = -2.99, $p$FDR $< 0.05$). No significant differences between groups for negative susceptibility values were observed for any other hippocampal ROI ($p$FDR $> 0.05$).

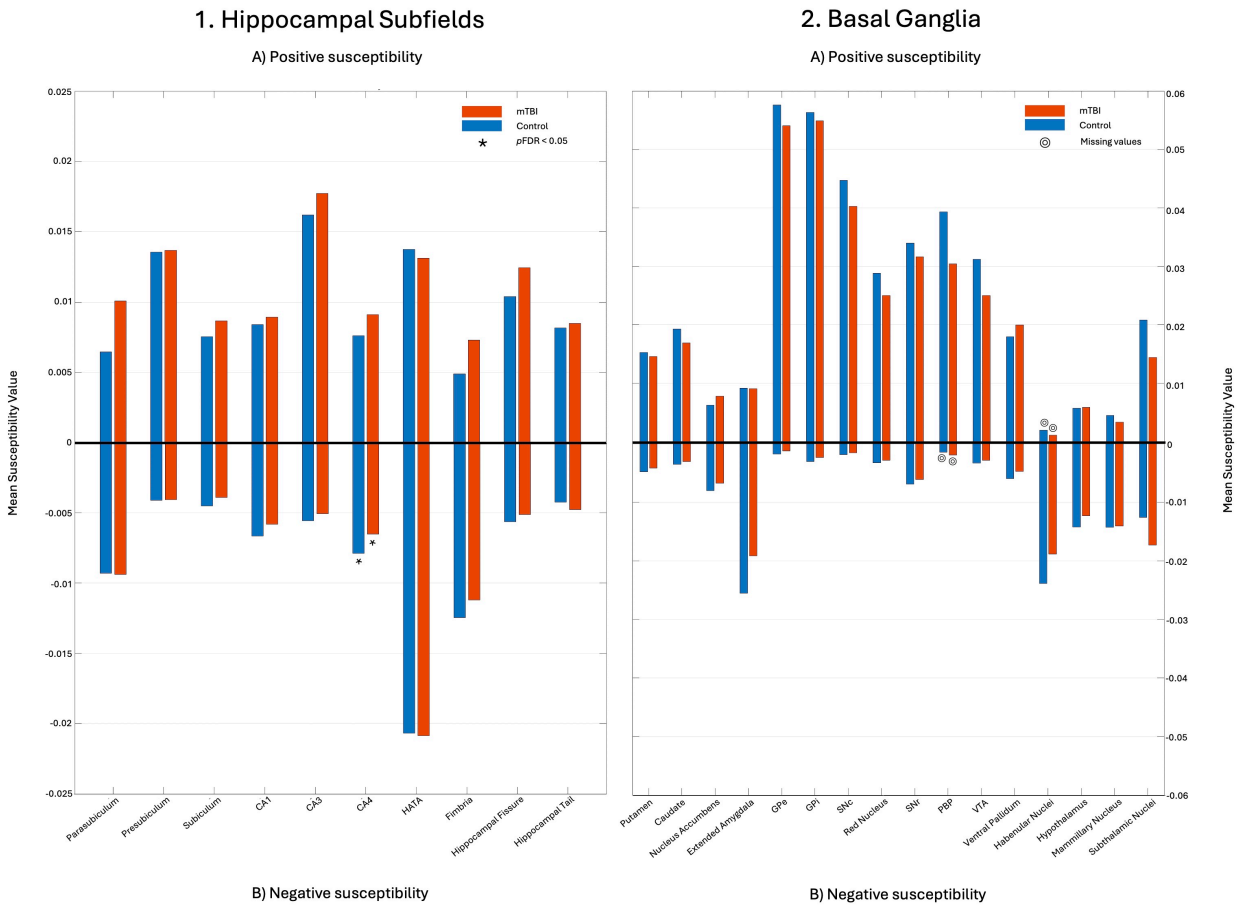


Fig 3: Mean susceptibility values in the hippocampal and basal ROIs

Bar plots showing the mean susceptibility values for mTBI (red bars) versus HC (blue bars) for: 1. Hippocampal Subfields, and; 2. Basal Ganglia, for both A) positive and B) negative susceptibility maps. Susceptibility is measured in ppm. ⋆ = significant differences between groups; ⊙ = regions omitted from further analysis due to zero ROI-wise values for any participant.

*Bilateral regional correlations*

Partial Pearson correlation coefficients were used to assess the relationship between age and both positive and negative susceptibility for the 10 hippocampal and 15 viable basal segmentations, controlling for group status. Additionally, correlations between both susceptibility signs and 1) BIST scores[60] as an indicator of injury severity, and; 2) DSI at the time of the MRI scan as a marker of injury latency, were conducted for the mTBI sample only. Negative susceptibility was transformed into absolute values to more clearly illustrate relationships between variables. P-values were adjusted for the 10 and 15 remaining segmentations for the hippocampal subfields and basal nuclei, respectively, using FDR procedures.[82]

*Age*

No statistically significant correlations were observed between age and positive susceptibility values for any hippocampal ROI, however, a significant positive correlation between age and absolute negative susceptibility in the fimbria ($r(48) = 0.42$, $p\text{FDR} < 0.05$) was observed, suggesting age-related increases in negative susceptibility (i.e., susceptibility becomes more negative with age) (see Fig. 4).

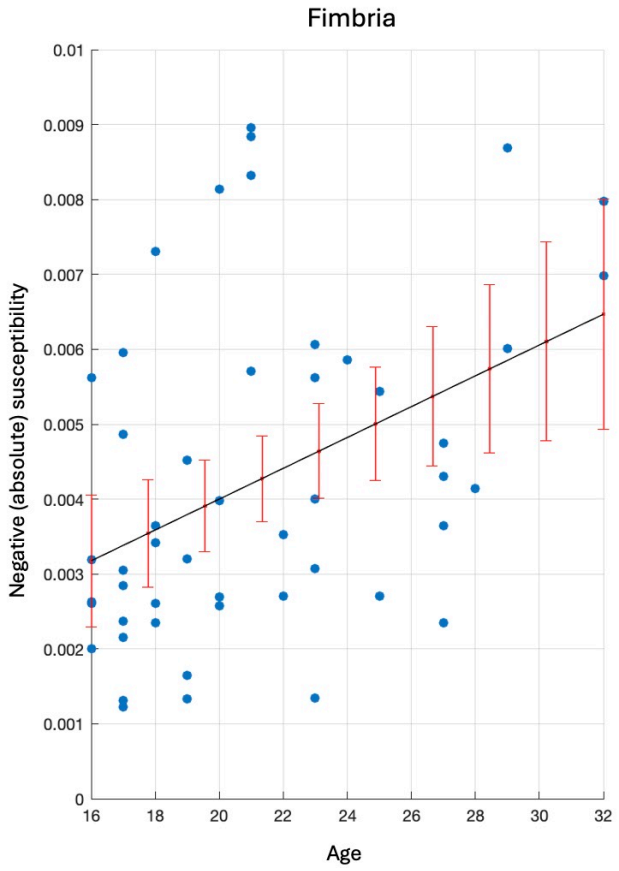


Fig 4: Significant correlations: Age and negative susceptibility in the fimbria

Scatter plot illustrating the statistically significant correlation between absolute negative (absolute) susceptibility values in the hippocampal fimbria and age. A line of best fit (black) highlights the trend. 95% confidence interval bars (red) indicate the predicted range for true values, providing a measure of uncertainty in the model.

Results indicated significant age-related increases in positive susceptibility values in several basal regions, including the putamen ($r(48) = 0.64$, $p\text{FDR} < 0.001$), caudate ($r(48) = 0.50$, $p\text{FDR} = 0.001$), red nucleus ($r(48) = 0.66$, $p\text{FDR} < 0.001$), PBP ($r(48) = 0.40$, $p\text{FDR} < 0.05$), and ventral pallidum ($r(48) = 0.35$, $p\text{FDR} < 0.05$) (see Fig. 5).

Significant positive correlations were also evident between age and absolute negative susceptibility in the caudate ($r(48) = 0.39$, $p\text{FDR} < 0.05$) and extended amygdala ($r(48) = 0.51$, $p\text{FDR} < 0.01$) suggesting that susceptibility in these regions tends to increase (become more negative) with age. Significant negative correlations were also observed between age and absolute negative susceptibility values in the ventral pallidum ($r(48) = -0.37$, $p\text{FDR} < 0.05$), suggesting that susceptibility tends to decrease (become less negative) with age (see Fig. 5).

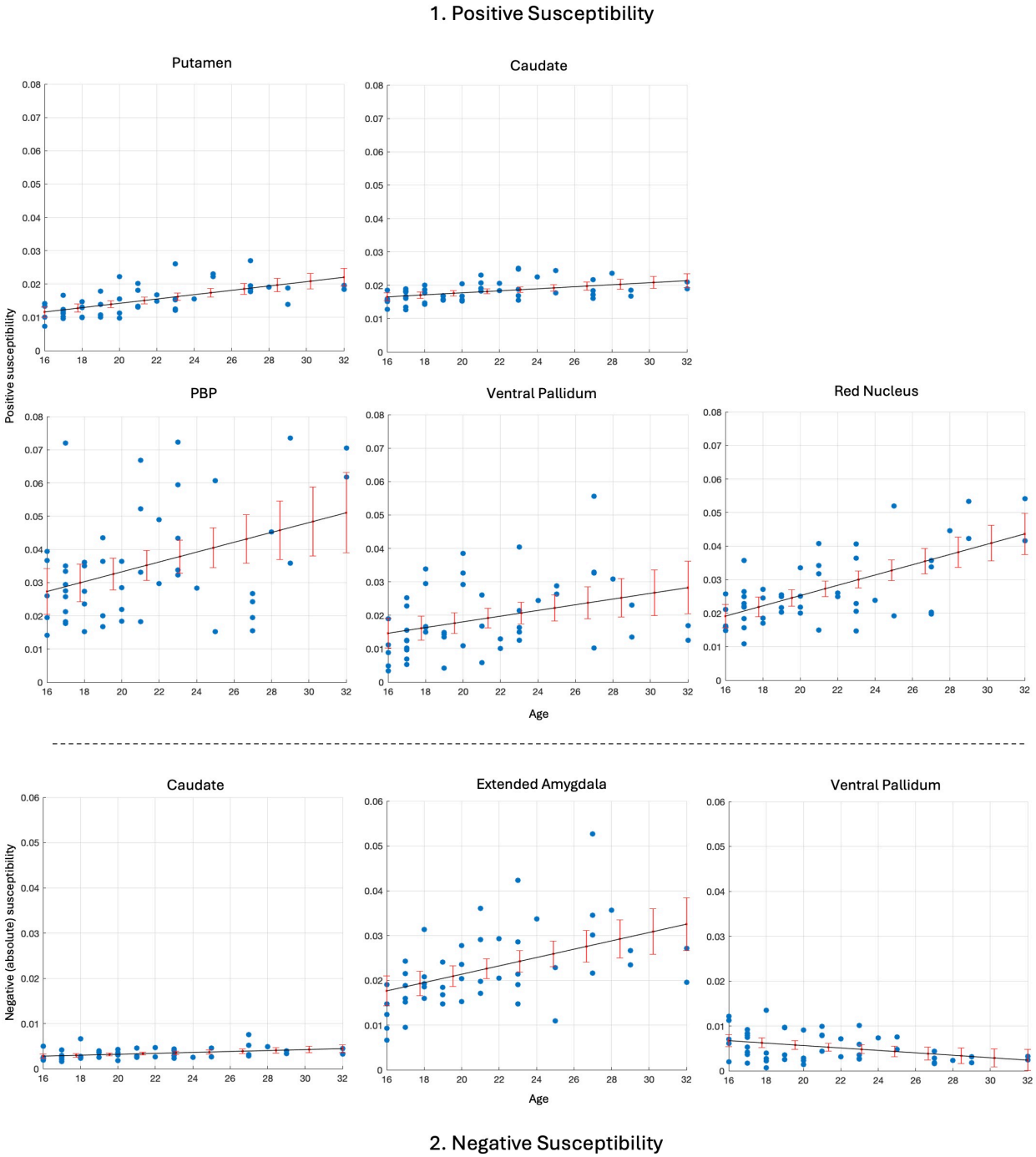


Fig 5: Significant correlations: Age and susceptibility values in the basal ganglia

Scatter plots illustrating the statistically significant correlations between both 1. Positive and 2. Negative (absolute) susceptibility values and age in basal ROIs. A line of best fit (black) highlights the trend. 95% confidence interval bars (red) indicate the predicted range for true values, providing a measure of uncertainty in the model.

*Injury severity and injury latency*

No statistically significant correlations were observed between both positive and negative absolute susceptibility sign and either DSI or BIST scores, for any basal or hippocampal nuclei ($p$FDR $> 0.05$).

## Discussion

Despite the vulnerability of the striatum and other deep nuclei to mechanical strain, cytoskeletal damage, and secondary metabolic disruptions after mTBI, all of which are risk factors for iron accumulation, previous QSM research has not yet achieved the anatomical specificity necessary to properly characterise mTBI-related alterations to tissue content in the subcortical grey matter. To address this limitation, we performed a highly detailed segmentation of the basal ganglia alongside the first QSM analysis of the distinct hippocampal subfields in mTBI. Magnetic source-separated QSM analyses were used to better represent mTBI effects on substrates with disparate biomagnetic profiles. Between-group comparisons showed no significant differences between mTBI participants and controls for either susceptibility sign in the basal ganglia, or for positive sign in the hippocampal subfields. However, the hippocampal CA4 region exhibited significantly decreased (less negative) negative susceptibility values for the mTBI group relative to healthy controls. Correlational analyses also revealed no significant associations between either susceptibility map and injury latency or severity in the mTBI group within any ROI. Congruent with expected age-related trends, positive susceptibility values in the putamen, caudate, PBP, ventral pallidum, and red nucleus increased with age. Age-related increases in negative susceptibility were also apparent in the hippocampal fimbria, the caudate, and the extended amygdala, but decreased with age in the ventral pallidum.

### *Diamagnetism is decreased in CA4 after mTBI*

The hippocampal CA4 region is particularly susceptible to both tau pathology in CTE,[57,83] which is considered a supporting feature for diagnosis,[84] and associated local dendritic swelling.[85] As a microtubule-associated protein, tau is considered a promising early indicator of axonal injury in mTBI.[86] While focal accumulation of tau would likely result in increased diamagnetism on QSM,[32,33] the observation of decreased diamagnetism in CA4 reported here nonetheless supports an axonal-injury model. This type of injury is characteristic of both TBI[87] and mTBI,[88] and is associated with disruptions of the myelin sheath[89,90] or demyelination as demonstrated in both animal models[91] and human QSM studies investigating sr-mTBI.[92] Although density of myelinated fibers is relatively low in the hilus (CA4),[93] disruptions to myelination in this region could plausibly account for localised decreases in negative susceptibility. Acute decreases in diagmagnetism indicative of myelin disruption focal to CA4 suggests this area could be vulnerable to axonal damage during mTBI. This damage could speculatively form the basis for development of an injury cascade that culminates in tauopathy as a downstream pathological event later in life for some people.

Other plausible explanations for decreased negative susceptibility after mTBI could be related to phagocytosis of stressed cells and their components, including myelin. Microglia and macrophages are known to target and phagocytose distressed but still viable cells, even in the absence of cell death.[94] This could result in a reduction in negative susceptibility if cells within a ROI are particularly sensitive to even mild injury and resultant distress signalling. Indeed, research suggests that the CA4 region is selectively vulnerable to sustained cell loss after blunt head injury.

### *Paramagnetic substrates in subcortical grey matter*

This, and other,[42–47] QSM investigations have found no significant evidence of iron accumulation in the basal nuclei or hippocampus after mTBI. However, iron accumulation as a pathologic feature of mTBI in many of these regions is well documented, contradicting the lack of iron-related findings reported here. For example; an iron-sensitive magnetic field correlation (MFC) study[37] reported notable iron accumulation in the globus pallidus and thalamus following mTBI. Investigations using susceptibility weighted imaging (SWI) have also identified iron deposition in the caudate, thalamus, right substantia nigra, red nucleus, lenticular nucleus, splenium of the corpus callosum, and hippocampus in chronic mTBI, concomitantly linking accumulations in the substantia nigra with cognitive dysfunction.[53] Studies using $T_2^*$ imaging have identified iron deposition in cortical,

subcortical (left putamen, bilateral hippocampal), and brainstem regions,[95] along with reports of accumulation in the lateral geniculate nucleus of the thalamus,[96] with both studies citing associations between elevated iron and post-mTBI headache symptomatology. Additionally, animal models of controlled cortical impact TBI have demonstrated iron deposition in the thalamus ipsilateral to the impact site upon histological examination, with focal depositions co-localising $T_2$ hypointensity on MRI.[97] Beyond acute pathological dyshomeostasis, post-mortem studies have provided evidence of iron accumulation in hippocampal neurofibrillary tangles (NFTs) in CTE,[59] as well as abnormal hemosiderin-laden macrophages near small vessels in the frontal and temporal lobes less than one year post-injury, indicating ferritin-bound non-heme iron deposition.[98]

Despite the previous research highlighting the vulnerability of the basal nuclei and hippocampus to iron-mediated pathology post-injury, an absence of significant group differences in positive susceptibility observed in this study may suggest a general protective effect conferred by the deep subcortical location of these regions. In contrast, our prior work has demonstrated that the cortex, particularly the parahippocampal gyrus, is susceptible to iron-mediated pathology following mTBI.[48] In more targeted, individualised analyses, cortical iron pathology has been observed in one-third of mTBI participants (rising to 83% when accounting for cortical depth and curvature) across various cortical ROIs, which was related to worse injury-related symptoms.[99]

It is also reasonable to suggest that the absence of between-group differences in iron markers may reflect the influence of normal age-related increases in iron (for a review, see Madden and Merenstein[17]), which could obscure subtle mTBI-specific effects. Age-related iron deposition is particularly pronounced in the basal nuclei and most evident within the age range of participants in this study, as discussed in more detail further below. This shared characteristic among younger individuals may explain the lack of significant group differences in iron-related markers. In contrast, the general lack of age effects in hippocampal regions and the resultant sensitivity to disruptions in diamagnetism in the CA4 region supports the hypothesis that changes to biomagnetism which are common to all participants may obscure injury-related susceptibility effects. Consequently, the unique alteration to diamagnetic hippocampal CA4 susceptibility is thus likely to reflect specific pathological consequences of mTBI. In keeping with these observations, the use of magnetic source separation likely enabled the isolation and identification of weaker diamagnetic effects, which might otherwise have been diluted or overshadowed by stronger positive susceptibility signals.[26] This could also account for the lack of significant differences reported in previous studies where source separation techniques were not employed,[42–47] providing support for a thresholded approach to QSM analysis.

*Diamagnetic substrates in subcortical grey matter*

We found no evidence of increased negative susceptibility in the subcortical grey matter following mTBI. However, alterations to varying biomagnetic substrates following TBI have previously been characterised in murine models using QSM and $R_2^*$ imaging alongside histological examinations to assess changes not only to iron, but also myelin and calcium.[100] These models have demonstrated concurrent iron and calcium accumulation, as well as demyelination after impact. These findings are reinforced by additional *in-vivo* and *ex-vivo* murine models of TBI also reporting significant calcifications, which are proposed as an indirect measure of inflammation[101] and microglia activation[102] following injury. Of particular interest, studies have noted that calcifications often co-localise with paramagnetic iron in TBI.[100] This finding underscores the complex interplay of tissue components affected by mTBI and highlights the contribution of both paramagnetic and diamagnetic substrates to injury pathology. This further validates the need for source separation in QSM research to accurately differentiate these overlapping effects and better elucidate underlying biological mechanisms.

A$\beta$ and tau, two proteins with potentially diamagnetic properties,[31–33] have been associated with both acute injury pathology and later neurodegenerative processes, and are known to co-localise with iron in Alzheimer's disease[17] and CTE.[59] Tau is a promising fluid biomarker for axonal injury in mTBI[86] and specific distributions of p-tau are considered pathognomonic of CTE, particularly in frontal and temporal cortices and hippocampal regions.[83,85] Fluid tau levels may be elevated acutely following TBI[103,104] and A$\beta$ can also accumulate within hours of TBI.[105] Focal accumulations may be present in the entorhinal cortex, hippocampus, and striatum (caudate and putamen) as evidenced by PET studies of TBI.[106] The aggregation of both proteins would likely produce differences in diamagnetism on QSM. However, systematic reviews have noted inconsistencies between studies regarding the presence or absence of A$\beta$ as a pathologic feature of TBI,[106] and similar conflicting evidence exists regarding the biodynamics of tau in mTBI, with some studies suggesting elevations within hours-to-days, and others indicating no difference between individuals with mTBI and controls acutely after injury.[86] These factors may have contributed to the absence of quantifiable increases in diamagnetism in the present study, particularly in so young a cohort[107,108] imaged at the acute stage of a mild head injury.

*Age-related differences in biomagnetic substrates*

Iron increases throughout the lifespan as a function of normal ageing.[17,109] Particularly steep increases in brain iron content are present in the red nucleus and substantia nigra within the first 20 years of life, the globus pallidus at approximately 30 years, with maximal values reached in the putamen and caudate at approximately 5 to six decades after birth.[35] These histological studies are supported by extensive QSM investigations,[17] for example; QSM and $R_2^*$ investigations have demonstrated susceptibility increases in the putamen and globus pallidus throughout adulthood, with deposition in the caudate peaking in the third decade.[110] Other QSM studies have evidenced increased susceptibility values in the caudate, putamen, globus pallidus, red nucleus, and substantia nigra in healthy older populations relative to younger samples.[111] Both imaging and histological studies support the biological plausibility of correlational results presented here, particularly within the caudate, putamen, and red nucleus.[17] This study also extends the existing literature through the observation of additional age-related positive susceptibility increases in the PBP and ventral pallidum. Our correlational findings, and evidence from the literature more broadly, suggest that a younger cohort is particularly prone to iron deposition as a shared characteristic, irrespective of mTBI status. For hippocampal regions, on the other hand, age-related iron accumulation apparent in previous research[17,109,112,113] was not reflected in the results of this study, potentially due to a likelihood of more subtle effects in these regions, coupled with the limited age range of this sample.

The temporal dynamics of diamagnetic substrates are relatively under-investigated in QSM, making inferences far less substantive than those related to paramagnetism and iron. Although myelin is presumed to be the main source of diamagnetism on QSM[27] it is unlikely that increases in diamagnetism reflect age-related increases in myelin content. Whilst developmental myelination of axons is apparent up until approximately 30 years of age, this protraction of normal processes is generally restricted to prefrontal cortical regions.[114] In other brain regions, steep increases in myelin content are most apparent in the first months of life, after which time any disparities between age groups are unlikely to produce noticeable differences in tissue contrast on MRI.[115] Age-related kinetics of A$\beta$ and tau aggregation point toward similar conclusions. While deposits of A$\beta$ have been detected in the brains of individuals as young as 20 years old,[116] it is typically a feature associated with older age, and has been noted in both the presence and absence of cognitive dysfunction;[107] a similar pattern to that of observed in tau accumulation.[108] As such, trends for increasing diamagnetism with age are unlikely to be related to proteinopathy. As a result, reasonable speculation suggests that the positive relationship between diamagnetism and age in the caudate, extended amygdala, and hippocampal fimbria may be related instead to calcifications in these regions. This is supported by a body of work highlighting age-related calcifications in the basal ganglia[117,118] and hippocampus[119] in healthy

individuals. However, the paucity of granular segmentations in the wider literature makes drawing parallels with the present research more difficult.

Conversely, the decrease in negative susceptibility as a function of age in the ventral pallidum may be related to myelin changes. The ventral pallidum contains both neuronal cell bodies and myelinated axons for rapid signal transmission.[120–122] Although literature related to age-induced demyelination specific to this region does not abound, investigations of myelin biodynamics more broadly suggests a 10% decrease per decade between the ages of 20 and 80,[123] which may account for the moderate effects evident here.

*Injury latency and severity*

While research suggests a negative correlation between iron deposition and cognitive ability following mTBI,[53] self-reported injury severity is often misaligned with objective markers of pathology, including on neuroimaging.[124,125] Alongside the under-reporting of symptoms that often occurs following a sr-mTBI,[126,127] these factors could confound results and contribute to the lack of correlation between positive or negative susceptibilities and both BIST scores and injury latency observed here. However, results from a previous investigation have suggested a link between injury severity and *cortical* iron dyshomeostasis.[99] The cortex is particularly vulnerable to a diverse range of injury mechanisms and downstream pathology in mTBI, including acute mechanical deformation and sulcal 'water hammer' injury, which may be implicated in cortical atrophy and tauopathy in CTE.[58,128,129] It is therefore not unreasonable to suggest that cortical, rather than subcortical, injury may be more predictive of adverse symptomatology after mTBI. Finally, mTBI-related neuropathology may be time-dependent, and more evident at subacute and chronic stages. Additional longitudinal research may be needed to better represent associations between injury latency and alterations to brain tissue content.

*Limitations*

The absence of elevations in paramagnetic or diamagnetic susceptibility following mTBI suggest that iron deposition, calcifications, or focal aggregation of proteins such as tau and A$\beta$ may not be present at the acute stage of injury. However, aforementioned research provides strong evidence that head injury more broadly, and even mild instances, can lead to diverse changes across biomagnetic substrates. Several factors may have inhibited the detection of changes in this research. Firstly, focal accumulations of iron, calcium, or proteins may better characterise chronic or later-life effects rather than acute pathophysiology, as evidenced by neuroimaging studies where differences in iron deposition were apparent at an average of 559 days post-injury.[37] Secondly, tau elevations are most commonly reported in cases of repeated exposure to head injuries[86] and tau oligomer polymorphisms are expressed differently in single versus repetitive mTBI.[130] However, in the absence of prior injury data, the study design precluded stratification of mTBI participants according to prior mTBI exposure. Without this information, detection of negative susceptibility changes and the potential relationship with tau pathology may be inhibited. Future studies should consider longitudinal research designs tracking athletes' exposure to head injury to better elucidate the cumulative and temporal effect of mTBI on kinetics of biomagnetic substrates. Additionally, notwithstanding the detail of the segmentations used in this study relative to previous more macroscopic investigations, the spatial resolution of the susceptibility maps may still limit detection of microstructural alterations. Because the susceptibility value at each voxel in a QSM image is obtained by convolving the susceptibilities of neighbouring voxels with a dipole kernel, each voxels susceptibility value is influenced by the surrounding susceptibility distribution,[131] and thus resolutions of 1 mm and above may hinder the detection of the subtle pathophysiological changes associated with mTBI. Additionally, the use of single-echo QSM restricted voxel thresholding to an inter-voxel approach. As a result, the presence of multiple biological substrates with opposing magnetic properties *within* voxels may have confounded results by representing an aggregate of all susceptibility sources. These bipolar contributions within voxels cannot be disambiguated, and thus analysed,

without multi-echo acquisitions.[132–134] This was also a likely cause of missing values in certain ROIs comprised primarily of either paramagnetic or diamagnetic susceptibility sources, such as the habenular nuclei or PBP (see Fig. 3). Thresholding these extremely polarised regions may result in zero values for the non-dominant sign for some participants, which may be further exacerbated by the size of ROIs, like the relatively small habenular nuclei. The use of multi-echo acquisitions would likely resolve this limitation also, and should be considered for future research using a thresholded approach. In addition, group-level analyses may obscure individual neuropathology and inter-individual heterogeneity[99,135,136] and less macroscopic statistical approaches are currently planned for future research. Lastly, this research was conducted on a sample exclusively comprised of males, limiting external validity. This is particularly relevant to the translation of findings reported here to female sports players. Sex can influence time-dependence of the neuroinflammatory response,[86] and fluctuating sex hormone profiles,[137] oral contraceptive use,[138] and variability in neck muscle morphology[139] can contribute to differences in injury severity and outcome. Further research is planned within this demographic, and will ensure generalisability to female athletes of this age range.

**Conclusions**

This research builds upon previous QSM studies of mTBI by presenting the first assessment of mild injury effects specifically in the hippocampal subfields, and offers the most detailed segmentation of the basal ganglia to date. Here, both positive (iron-related) and negative (myelin-, calcium-, and protein-related) susceptibility maps were utilised to better understand the impact of mTBI on biological substrates with differing biomagnetic profiles. Results revealed mTBI-related decreased negative susceptibility in the hippocampal CA4, indicating potential disruption to the myelin sheaths of neurons in this region which may represent a component of the degenerative injury cascade leading to local tauopathy in CTE. The absence of significant increases in either susceptibility sign as a marker of mTBI pathophysiology may reflect a general protective effect of sub-cortical location within the brain, or the confounding effect of age-related susceptibility changes common to all participants. Finally, results from correlational analyses support and extend prior literature regarding age-related iron deposition in subcortical grey matter and contributes to the sparse literature on the relationship between diamagnetic tissue content and age.

**Author Contributions**

**Christi A. Essex** (Conceptualisation, Methodology, Project Administration, Validation, Software, Formal Analysis, Investigation, Resources, Data Curation, Writing - Original Draft, Writing - Review & Editing, Visualisation); **Mayan J. Bedggood** (Writing - Review & Editing, Project administration, Investigation); **Jenna L. Merenstein** (Writing - Review & Editing); **Catherine Morgan** (Methodology, Writing - Review & Editing); **Helen Murray** (Writing - Review & Editing); **Samantha J. Holdsworth** (Writing - Review & Editing); **Richard L.M. Faull** (Writing - Review & Editing); **Patria Hume** (Writing - Review & Editing); **Alice Theadom** (Conceptualisation, Methodology, Writing - Review & Editing, Funding acquisition, Supervision); **Mangor Pedersen** (Conceptualisation, Methodology, Writing - Review & Editing, Funding acquisition, Supervision)

**Acknowledgements**

We extend thanks to Amabelle Voice-Powell and Cassandra McGregor for their contribution to the data collection, and Tania Ka'ai for bringing her perspective to cultural considerations on this study. In addition, we thank Axis Sports Concussion Clinics, particularly Dr Stephen Kara, for their assistance with recruiting sr-mTBI participants and personnel at the Centre for Advanced Magnetic Resonance Imaging (CAMRI) for their assistance collecting MRI data. We also acknowledge Dr Tim Elliot for radiological reporting of all participants and Siemens Healthineers for the use of a work-in-progress (WIP) prototype sequence for the acquisition data used to perform QSM.

**Funding**

This project was funded by a grant from the Health Research Council of New Zealand (HRC), grant #21/622.

The first author (CE) is supported by a Dame Dorothy Winstone Doctoral Completion Award from the Kate Edger Foundation of New Zealand.

**Competing Interests**

The authors report no competing interests.

**Data availability**

De-identified MRI data and code used for image processing and statistical analysis can be made available upon request to the corresponding author.

**References**


1 A. I. Maas, D. K. Menon, G. T. Manley, *et al.*, "Traumatic brain injury: progress and challenges in prevention, clinical care, and research," *The Lancet Neurology* **21**, 1004–1060 (2022).

2 A. Theadom, S. Mahon, P. Hume, *et al.*, "Incidence of Sports-Related Traumatic Brain Injury of All Severities: A Systematic Review," *Neuroepidemiology* **54**(2), 192–199 (2020).

3 K. McInnes, C. L. Friesen, D. E. MacKenzie, *et al.*, "Mild Traumatic Brain Injury (mTBI) and chronic cognitive impairment: A scoping review," *PLoS ONE* **12** (2017).

4 L. De Beaumont, H. Thoret, D. Mongeon, *et al.*, "Brain function decline in healthy retired athletes who sustained their last sports concussion in early adulthood," *Brain* **132**(3), 695–708 (2009).

5 K. M. Guskiewicz, S. W. Marshall, J. Bailes, *et al.*, "Association between Recurrent Concussion and Late-Life Cognitive Impairment in Retired Professional Football Players," *Neurosurgery* **57**(4), 719–726 (2005).

6 S. C. Hellewell, C. S. Beaton, T. Welton, *et al.*, "Characterizing the risk of depression following mild traumatic brain injury: A meta-analysis of the literature comparing chronic mTBI to non-mTBI populations," *Frontiers in Neurology* **11**, 1–14 (2020).

7 K. M. Guskiewicz, S. W. Marshall, J. Bailes, *et al.*, "Recurrent concussion and risk of depression in retired professional football players," *Medicine and Science in Sports and Exercise* **39**(6), 903–909 (2007).

8 D. F. Mackay, E. R. Russell, K. Stewart, *et al.*, "Neurodegenerative Disease Mortality among Former Professional Soccer Players," *New England Journal of Medicine* **381**(19), 1801–1808 (2019).

9 Y. Naumenko, I. Yuryshinetz, Y. Zabenko, *et al.*, "Mild traumatic brain injury as a pathological process," (2023).

10 C. B. Jeter, G. W. Hergenroeder, M. J. Hylin, *et al.*, "Biomarkers for the diagnosis and prognosis of mild traumatic brain injury/concussion," *Journal of Neurotrauma* **30**, 657–670 (2013).

11 A. Gozt, S. Hellewell, P. G. Ward, *et al.*, "Emerging Applications for Quantitative Susceptibility Mapping in the Detection of Traumatic Brain Injury Pathology," *Neuroscience* **467**, 218–236 (2021).

12 M. Prins, T. Greco, D. Alexander, *et al.*, "The pathophysiology of traumatic brain injury at a glance," *DMM Disease Models and Mechanisms* **6**, 1307–1315 (2013).

13 K. E. Saatman, A. C. Duhaime, R. Bullock, *et al.*, "Classification of traumatic brain injury for targeted therapies," in *Journal of Neurotrauma*, **25**, 719–738 (2008).

14 T. Seifert and V. Shipman, "The Pathophysiology of Sports Concussion," *Current Pain and Headache Reports* **19**(8) (2015).

15 K. R. Walker and G. Tesco, "Molecular mechanisms of cognitive dysfunction following traumatic brain injury," *Frontiers in Aging Neuroscience* **5** (2013).

16 C. C. Giza and D. A. Hovda, "The new neurometabolic cascade of concussion," *Neurosurgery* **75**, S24–S33 (2014).

17 D. J. Madden and J. L. Merenstein, "Quantitative susceptibility mapping of brain iron in healthy aging and cognition," *NeuroImage* **282** (2023).

18 R. J. Ward, F. A. Zucca, J. H. Duyn, *et al.*, "The role of iron in brain ageing and neurodegenerative disorders," *The Lancet Neurology* **13**(10), 1045–1060 (2014).

19 S. Huang, S. Li, H. Feng, *et al.*, "Iron Metabolism Disorders for Cognitive Dysfunction After Mild Traumatic Brain Injury," *Frontiers in Neuroscience* **15** (2021).

20 H. Ma, Y. Dong, Y. Chu, *et al.*, "The mechanisms of ferroptosis and its role in alzheimer's disease," *Frontiers in Molecular Biosciences* **9** (2022).

21 E. L. Mackenzie, K. Iwasaki, and Y. Tsuji, "Intracellular iron transport and storage: From molecular mechanisms to health implications," *Antioxidants and Redox Signaling* **10**(6), 997–1030 (2008).

22 E. J. Nisenbaum, D. S. Novikov, and Y. W. Lui, "The presence and role of iron in mild traumatic brain injury: An imaging perspective," *Journal of Neurotrauma* **31**, 301–307 (2014).

23 J. H. Duyn and J. Schenck, "Contributions to magnetic susceptibility of brain tissue," *NMR in Biomedicine* **30**(4) (2017).

24 C. Langkammer, F. Schweser, N. Krebs, *et al.*, "Quantitative susceptibility mapping (QSM) as a means to measure brain iron? A post mortem validation study," *NeuroImage* **62**(3), 1593–1599 (2012).

25 C. Liu, W. Li, K. A. Tong, *et al.*, "Susceptibility-weighted imaging and quantitative susceptibility mapping in the brain," *Journal of Magnetic Resonance Imaging* **42**(1), 23–41 (2015).

26 P. Ravanfar, S. M. Loi, W. T. Syeda, *et al.*, "Systematic Review: Quantitative Susceptibility Mapping (QSM) of Brain Iron Profile in Neurodegenerative Diseases," *Frontiers in Neuroscience* **15** (2021).

27 K. Deh, G. D. Ponath, Z. Molvi, *et al.*, "Magnetic susceptibility increases as diamagnetic molecules breakdown: Myelin digestion during multiple sclerosis lesion formation contributes to increase on QSM," *Journal of Magnetic Resonance Imaging* **48**, 1281–1287 (2018).

28 J. Jang, Y. Nam, S. W. Jung, *et al.*, "Paradoxical paramagnetic calcifications in the globus pallidus: An ex vivo MR investigation and histological validation study," *NMR in Biomedicine* **34**(10) (2021).

29 S. Kim, Y. Lee, C. Y. Jeon, *et al.*, "Quantitative magnetic susceptibility assessed by 7T magnetic resonance imaging in Alzheimer's disease caused by streptozotocin administration," *Quantitative Imaging in Medicine and Surgery* **10**(3), 789–797 (2020).

30 Y. Wang, P. Spincemaille, Z. Liu, *et al.*, "Clinical quantitative susceptibility mapping (QSM): Biometal imaging and its emerging roles in patient care," *Journal of Magnetic Resonance Imaging* **46**(4), 951–971 (2017).

31 N. J. Gong, R. Dibb, M. Bulk, *et al.*, "Imaging beta amyloid aggregation and iron accumulation in Alzheimer's disease using quantitative susceptibility mapping MRI," *NeuroImage* **191**, 176–185 (2019).

32 J. O'Callaghan, H. Holmes, N. Powell, *et al.*, "Tissue magnetic susceptibility mapping as a marker of tau pathology in Alzheimer's disease," *NeuroImage* **159**, 334–345 (2017).

33 Z. Zhao, L. Zhang, Q. Wen, *et al.*, "The effect of beta-amyloid and tau protein aggregations on magnetic susceptibility of anterior hippocampal laminae in Alzheimer's diseases," *NeuroImage* **244** (2021).

34 M. Daglas and P. A. Adlard, "The Involvement of Iron in Traumatic Brain Injury and Neurodegenerative Disease," *Frontiers in Neuroscience* **12** (2018).

35 B. Hallgren and P. Sourander, "The effect of age on the non-haemin iron in the human brain," *Journal of Neurochemistry* **3**, 41–51 (1958).

36 M. E. Haacke, N. Y. Cheng, M. J. House, *et al.*, "Imaging iron stores in the brain using magnetic resonance imaging," *Magnetic Resonance Imaging* **23**(1), 1–25 (2005).

37 E. Raz, J. H. Jensen, Y. Ge, *et al.*, "Brain iron quantification in mild traumatic brain injury: A magnetic field correlation study," *American Journal of Neuroradiology* **32**(10), 1851–1856 (2011).

38 J. Lifshitz, B. J. Kelley, and J. T. Povlishock, "Perisomatic Thalamic Axotomy After Diffuse Traumatic Brain Injury Is Associated With Atrophy Rather Than Cell Death," *J Neuropathol Exp Neurol* **66**(3), 218–229 (2007).

39 A. H. Ropper and K. C. Gorson, "Clinical practice. concussion," *The New England Journal of Medicine* **356**(2), 166–172 (2007).

40 N. A. Shaw, "The neurophysiology of concussion," *Progress in Neurobiology* **67**, 281–344 (2002).

41 K. M. Koch, A. S. Nencka, B. Swearingen, *et al.*, "Acute Post-Concussive Assessments of Brain Tissue Magnetism Using Magnetic Resonance Imaging," *Journal of Neurotrauma* **38**(7), 848–857 (2021).

42 D. K. Wright, T. J. O'Brien, and S. R. Shultz, "Sub-acute Changes on MRI Measures of Cerebral Blood Flow and Venous Oxygen Saturation in Concussed Australian Rules Footballers," *Sports Medicine - Open* **8**(1) (2022).

43 T. K. Bell, M. Ansari, J. M. Joyce, *et al.*, "Quantitative susceptibility mapping in adults with persistent-post concussion symptoms after mild traumatic brain injury: An exploratory study," *American Journal of Neuroradiology* (2024).

44 N. J. Gong, S. Kuzminski, M. Clark, *et al.*, "Microstructural alterations of cortical and deep gray matter over a season of high school football revealed by diffusion kurtosis imaging," *Neurobiology of Disease* **119**, 79–87 (2018).

45 N. N. Pinky, C. T. Debert, S. P. Dukelow, *et al.*, "Multimodal magnetic resonance imaging of youth sport-related concussion reveals acute changes in the cerebellum, basal ganglia, and corpus callosum that resolve with recovery," *Frontiers in Human Neuroscience* **16** (2022).

46 K. M. Koch, T. B. Meier, R. Karr, *et al.*, "Quantitative susceptibility mapping after sports-related concussion," *American Journal of Neuroradiology* **39**(7), 1215–1221 (2018).

47 R. Zivadinov, P. Polak, F. Schweser, *et al.*, "Multimodal Imaging of Retired Professional Contact Sport Athletes Does Not Provide Evidence of Structural and Functional Brain Damage," *Journal of Head Trauma Rehabilitation* **33**(5), E24–E32 (2018).

48 C. A. Essex, J. L. Merenstein, D. K. Overson, *et al.*, "Distribution of paramagnetic and diamagnetic cortical substrates following mild Traumatic Brain Injury: A depth-and curvature-based quantitative susceptibility mapping study," *medRxiv* (Preprint) (2024).

49 P. Calabresi, B. Picconi, A. Tozzi, *et al.*, "Direct and indirect pathways of basal ganglia: A critical reappraisal," *Nature Neuroscience* **17**(8), 1022–1030 (2014).

50 L. Pessoa, "A Network Model of the Emotional Brain," *Trends in Cognitive Sciences* **21**(5), 357–371 (2017).

51 C. A. Seger, "The basal ganglia in human learning," *Neuroscientist* **12**(4), 285–290 (2006).

52 C. M. Bird and N. Burgess, "The hippocampus and memory: Insights from spatial processing," *Nature Reviews Neuroscience* **9**(3), 182–194 (2008).

53 L. Lu, H. Cao, X. Wei, *et al.*, "Iron Deposition Is Positively Related to Cognitive Impairment in Patients with Chronic Mild Traumatic Brain Injury: Assessment with Susceptibility Weighted Imaging," *BioMed Research International* **2015** (2015).

54 H. Arciniega, Z. H. Baucom, F. Tuz-Zahra, *et al.*, "Brain morphometry in former American football players: 1 findings from the DIAGNOSE CTE research project," *Oxford University Press* **22** (2024).

55 F. D. Raslau, I. T. Mark, A. P. Klein, *et al.*, "Memory Part 2: The Role of the Medial Temporal Lobe," *American Journal of Neuroradiology* **36**, 846–849 (2015).

56 A. C. Mckee and D. H. Daneshvar, "The neuropathology of traumatic brain injury," in *Handbook of Clinical Neurology*, **127**, 45–66, Elsevier B.V. (2015).

57 J. D. Cherry, C. D. Esnault, Z. H. Baucom, *et al.*, "Tau isoforms are differentially expressed across the hippocampus in chronic traumatic encephalopathy and Alzheimer's disease," *Acta Neuropathologica Communications* **9** (2021).

58 A. C. McKee, T. D. Stein, B. R. Huber, *et al.*, "Chronic traumatic encephalopathy (CTE): criteria for neuropathological diagnosis and relationship to repetitive head impacts," *Acta Neuropathologica* **145**(4), 371–394 (2023).

59 C. Bouras, P. Giannakopoulos, P. F. Good, *et al.*, "A Laser Microprobe Mass Analysis of Brain Aluminum and Iron in Dementia pugilistica: Comparison with Alzheimer's Disease," *Eur Neurol* **38**(1), 53–58 (1997).

60 A. Theadom, N. Hardaker, C. Bray, *et al.*, "The Brain Injury Screening Tool (BIST): Tool development, factor structure and validity," *PLoS ONE* **16**(2 February) (2021).

61 K. J. Gorgolewski, T. Auer, V. D. Calhoun, *et al.*, "The brain imaging data structure, a format for organizing and describing outputs of neuroimaging experiments," *Scientific Data* **3** (2016).

62 A. Boré, S. Guay, C. Bedetti, *et al.*, "Dcm2Bids," (2023).

63 X. Li, P. S. Morgan, J. Ashburner, *et al.*, "The first step for neuroimaging data analysis: DICOM to NIfTI conversion," *Journal of Neuroscience Methods* **264**, 47–56 (2016).

64 A. W. Stewart and S. Bollman, "QSMxT/QSMxT," (2022).

65 A. W. Stewart, S. D. Robinson, K. O'Brien, *et al.*, "QSMxT: Robust masking and artifact reduction for quantitative susceptibility mapping," *Magnetic Resonance in Medicine* **87**(3), 1289–1300 (2022).

66 B. Dymerska, K. Eckstein, B. Bachrata, *et al.*, "Phase unwrapping with a rapid opensource minimum spanning tree algorithm (ROMEO)," *Magnetic Resonance in Medicine* **85**(4), 2294–2308 (2021).

67 T. Liu, I. Khalidov, L. de Rochefort, *et al.*, "A novel background field removal method for MRI using projection onto dipole fields (PDF)," *NMR in Biomedicine* **24**(9), 1129–1136 (2011).

68 C. Kames, V. Wiggermann, and A. Rauscher, "Rapid two-step dipole inversion for susceptibility mapping with sparsity priors," *NeuroImage* **167**, 276–283 (2018).

69 B. Bilgic, M. Costagli, K.-S. Chan, *et al.*, "Recommended Implementation of Quantitative Susceptibility Mapping for Clinical Research in The Brain: A Consensus of the ISMRM Electro-Magnetic Tissue Properties Study Group," tech. rep., QSM Consensus Organization Committee (2023).

70 S. M. Smith, "Fast robust automated brain extraction," *Human Brain Mapping* **17**(3), 143–155 (2002).

71 W. M. Pauli, A. N. Nili, and J. Michael Tyszka, "Data Descriptor: A high-resolution probabilistic in vivo atlas of human subcortical brain nuclei," *Scientific Data* **5** (2018).

72 D. N. Greve and B. Fischl, "Accurate and robust brain image alignment using boundary-based registration," *NeuroImage* **48**(1), 63–72 (2009).

73 M. Jenkinson, P. Bannister, M. Brady, *et al.*, "Improved Optimization for the Robust and Accurate Linear Registration and Motion Correction of Brain Images," *NeuroImage* **17**(2), 825–841 (2002).

74 M. Jenkinson and S. Smith, "A global optimisation method for robust affine registration of brain images," *Medical Image Analysis* **5**, 143–156 (2001).

75 J. L. Merenstein, J. Zhao, D. K. Overson, *et al.*, "Depth- and curvature-based quantitative susceptibility mapping analyses of cortical iron in Alzheimer's disease," *Cerebral Cortex* **34**(2) (2024).

76 J. R. Reichenbach, "The future of susceptibility contrast for assessment of anatomy and function," *NeuroImage* **62**(2), 1311–1315 (2012).

77 N. J. Tustison, B. B. Avants, P. A. Cook, *et al.*, "N4ITK: Improved N3 bias correction," *IEEE Transactions on Medical Imaging* **29**(6), 1310–1320 (2010).

78 B. B. Avants, N. J. Tustison, G. Song, *et al.*, "A reproducible evaluation of ANTs similarity metric performance in brain image registration," *NeuroImage* **54**(3), 2033–2044 (2011).

79 B. Fischl, "FreeSurfer," (2012).

80 J. E. Iglesias, J. C. Augustinack, K. Nguyen, *et al.*, "A computational atlas of the hippocampal formation using ex vivo, ultra-high resolution MRI: Application to adaptive segmentation of in vivo MRI," *Neuroimage* (115), 117–137 (2015).

81 D. J. Tournier, R. Smith, D. Raffelt, *et al.*, "MRtrix3: A fast, flexible and open software framework for medical image processing and visualisation," *NeuroImage* **202** (2019).

82 Y. Benjamini and Y. Hochberg, "Controlling the False Discovery Rate: A Practical and Powerful Approach to MultipleTesting," *Journal of the Royal Statistical Society. Series B (Methodological)* **57**(1), 289–300 (1995).

83 H. C. Murray, C. Osterman, P. Bell, *et al.*, "Neuropathology in chronic traumatic encephalopathy: a systematic review of comparative post-mortem histology literature," *Acta Neuropathologica Communications* **10**(1) (2022).

84 K. F. Bieniek, N. J. Cairns, J. F. Crary, *et al.*, "The Second NINDS/NIBIB Consensus Meeting to Define Neuropathological Criteria for the Diagnosis of Chronic Traumatic Encephalopathy," *Journal of Neuropathology and Experimental Neurology* **80**, 210–219 (2021).

85 A. C. McKee, N. J. Cairns, D. W. Dickson, *et al.*, "The first NINDS/NIBIB consensus meeting to define neuropathological criteria for the diagnosis of chronic traumatic encephalopathy," *Acta Neuropathologica* **131**(1), 75–86 (2016).

86 W. P. Flavin, H. Hosseini, J. W. Ruberti, *et al.*, "Traumatic brain injury and the pathways to cerebral tau accumulation," *Frontiers in Neurology* **14** (2023).

87 V. E. Johnson, W. Stewart, and D. H. Smith, "Axonal pathology in traumatic brain injury," *Experimental Neurology* **246**, 35–43 (2013).

88 M. Inglese, S. Makani, G. Johnson, *et al.*, "Diffuse axonal injury in mild traumatic brain injury: a diffusion tensor imaging study," *J. Neurosurg* **103**, 298–303 (2005).

89 W. L. Maxwell, A. Domleo, G. Mccoll, *et al.*, "Post-Acute Alterations in the Axonal Cytoskeleton after Traumatic Axonal Injury," *JOURNAL OF NEUROTRAUMA* **20**(2) (2003).

90 W. L. Maxwell, R. Kosanlavit, B. J. Mccreath, *et al.*, "Freeze-Fracture and Cytochemical Evidence for Structural and Functional Alteration in the Axolemma and Myelin Sheath of Adult Guinea Pig Optic Nerve Fibers After Stretch Injury," *Journal of Neurotrauma* **16**(4) (1999).

91 H. M. Bramlett and W. D. Dietrich, "Quantitative structural changes in white and gray matter 1 year following traumatic brain injury in rats," *Acta Neuropathologica* **103**(6), 607–614 (2002).

92 A. M. Weber, A. Pukropski, C. Kames, *et al.*, "Pathological insights from quantitative susceptibility mapping and diffusion tensor imaging in ice hockey players pre and post-concussion," *Frontiers in Neurology* **9** (2018).

93 H. Ábrahám, A. Vincze, I. Jewgenow, *et al.*, "Myelination in the human hippocampal formation from midgestation to adulthood," *International Journal of Developmental Neuroscience* **28**, 401–410 (2010).

94 F. Yu, Y. Wang, A. R. Stetler, *et al.*, "Phagocytic microglia and macrophages in brain injury and repair," *CNS Neuroscience and Therapeutics* **28**(9), 1279–1293 (2022).

95 S. Nikolova, T. J. Schwedt, J. Li, *et al.*, "T2* reduction in patients with acute post-traumatic headache," *Cephalalgia* **42**(4-5), 357–365 (2022).

96 C. D. Chong, S. Nikolova, G. Dumkrieger, *et al.*, "Thalamic subfield iron accumulation after acute mild traumatic brain injury as a marker of future post-traumatic headache intensity," *Headache* **63**, 156–164 (2023).

97 G. Onyszchuk, S. M. LeVine, W. M. Brooks, *et al.*, "Post-acute pathological changes in the thalamus and internal capsule in aged mice following controlled cortical impact injury: A magnetic resonance imaging, iron histochemical, and glial immunohistochemical study," *Neuroscience Letters* **452**, 204–208 (2009).

98 E. D. Bigler, "Neuropsychological results and neuropathological findings at autopsy in a case of mild traumatic brain injury," *Journal of the International Neuropsychological Society* (10), 794–806 (2004).

99 C. A. Essex, D. K. Overson, J. L. Merenstein, *et al.*, "Cortical iron-related markers are elevated in mild Traumatic Brain Injury: An individual-level quantitative susceptibility mapping study," *medRxiv* (Preprint) (2024).

100 K. Chary, M. J. Nissi, O. Nykänen, *et al.*, "Quantitative susceptibility mapping of the rat brain after traumatic brain injury," *NMR in Biomedicine* **34** (2021).

101 L. J. Lehto, A. Sierra, C. A. Corum, *et al.*, "Detection of calcifications in vivo and ex vivo after brain injury in rat using SWIFT," *NeuroImage* **61**, 761–772 (2012).

102 M. J. Gayoso, A. Al-Majdalawi, M. Garrosa, *et al.*, "Selective calcification of rat brain lesions caused by systemic administration of kainic acid," *Histology and Histopathology* (18), 855–869 (2003).

103 M. Ost, K. Nylén, L. Csajbok, *et al.*, "Initial CSF total tau correlates with 1-year outcome in patients with traumatic brain injury," *Neurology* **9**(69), 1600–1604 (2006).

104 R. Rubenstein, B. Chang, J. K. Yue, *et al.*, "Comparing plasma phospho tau, total tau, and phospho tau–total tau ratio as acute and chronic traumatic brain injury biomarkers," *JAMA Neurology* **74**, 1063–1072 (2017).

105 V. E. Johnson, W. Stewart, and D. H. Smith, "Traumatic brain injury and amyloid-$\beta$ pathology: A link to alzheimer's disease?," *Nature Reviews Neuroscience* **11**(5), 361–370 (2010).

106 K. M. Dybing, C. J. Vetter, D. A. Dempsey, *et al.*, "Traumatic brain injury and Alzheimer's Disease biomarkers: A systematic review of findings from amyloid and tau positron emission tomography (PET)," *medRxiv* (Preprint) (2023).

107 K. M. Rodrigue, K. M. Kennedy, and D. C. Park, "Beta-amyloid deposition and the aging brain," *Neuropsychology Review* **19**(4), 436–450 (2009).

108 M. Schöll, S. N. Lockhart, D. R. Schonhaut, *et al.*, "PET Imaging of Tau Deposition in the Aging Human Brain," *Neuron* **89**, 971–982 (2016).

109 A. Ashraf, M. Clark, and P. W. So, "The aging of iron man," *Frontiers in Aging Neuroscience* **10** (2018).

110 S. Treit, N. Naji, P. Seres, *et al.*, "R2* and quantitative susceptibility mapping in deep gray matter of 498 healthy controls from 5 to 90 years," *Human Brain Mapping* **42**, 4597–4610 (2021).

111 B. Bilgic, A. Pfefferbaum, T. Rohlfing, *et al.*, "MRI estimates of brain iron concentration in normal aging using quantitative susceptibility mapping," *NeuroImage* **59**(3), 2625–2635 (2012).

112 J. Hagemeier, J. J. Geurts, and R. Zivadinov, "Brain iron accumulation in aging and neurodegenerative disorders," *Expert Review of Neurotherapeutics* **12**(12), 1467–1480 (2012).

113 L. Zecca, M. B. Youdim, P. Riederer, *et al.*, "Iron, brain ageing and neurodegenerative disorders," *Nature Reviews Neuroscience* **5**(11), 863–873 (2004).

114 M. C. Moulson and C. A. Nelson, *Encyclopedia of Infant and Early Childhood Development: Neurological Development*, Elsevier (2008).

115 H. M. Branson, "Normal Myelination. A Practical Pictorial Review," *Neuroimaging Clinics of North America* **23**(2), 183–195 (2013).

116 A. Baker-Nigh, S. Vahedi, E. G. Davis, *et al.*, "Neuronal amyloid-$\beta$ accumulation within cholinergic basal forebrain in ageing and Alzheimer's disease," *Brain* **138**, 1722–1737 (2015).

117 E. Monfrini, F. Arienti, P. Rinchetti, *et al.*, "Brain Calcifications: Genetic, Molecular, and Clinical Aspects," *International journal of molecular sciences* **24**(10) (2023).

118 C. Saade, E. Najem, K. Asmar, *et al.*, "Intracranial calcifications on CT: An updated review," *Journal of Radiology Case Reports* **13**, 1–18 (2019).

119 J. Wegiel, I. Kuchna, T. Wisniewski, *et al.*, "Vascular fibrosis and calcification in the hippocampus in aging, Alzheimer disease, and Down syndrome," *Acta Neuropathologica* **103**(4), 333–343 (2002).

120 L. Heimer and G. W. Van Hoesen, "The limbic lobe and its output channels: Implications for emotional functions and adaptive behavior," *Neuroscience and Biobehavioral Reviews* **30**(2), 126–147 (2006).

121 Y. M. Kupchik and P. W. Kalivas, "The Direct and Indirect Pathways of the Nucleus Accumbens are not what you think," *Neuropsychopharmacology* **42**, 368–370 (2017).

122 D. H. Root, R. I. Melendez, L. Zaborszky, *et al.*, "The ventral pallidum: Subregion-specific functional anatomy and roles in motivated behaviors," *Progress in Neurobiology* **130**, 29–70 (2015).

123 L. Marner, J. R. Nyengaard, Y. Tang, *et al.*, "Marked loss of myelinated nerve fibers in the human brain with age," *Journal of Comparative Neurology* **462**(2), 144–152 (2003).

124 M. McCrea, T. Meier, D. Huber, *et al.*, "Role of advanced neuroimaging, fluid biomarkers and genetic testing in the assessment of sport-related concussion: A systematic review," *British Journal of Sports Medicine* **51**(12), 919–929 (2017).

125 M. E. Shenton, H. M. Hamoda, J. S. Schneiderman, *et al.*, "A review of magnetic resonance imaging and diffusion tensor imaging findings in mild traumatic brain injury," *Brain Imaging and Behavior* **6**(2), 137–192 (2012).

126 E. Kroshus, B. Garnett, M. Hawrilenko, *et al.*, "Concussion under-reporting and pressure from coaches, teammates, fans, and parents," *Social Science and Medicine* **134**, 66–75 (2015).

127 T. B. Meier, B. J. Brummel, R. Singh, *et al.*, "The underreporting of self-reported symptoms following sports-related concussion," *Journal of Science and Medicine in Sport* **18**, 507–511 (2015).

128 S. Kornguth, N. Rutledge, G. Perlaza, *et al.*, "A Proposed Mechanism for Development of CTE Following Concussive Events: Head Impact, Water Hammer Injury, Neurofilament Release, and Autoimmune Processes," *Brain Sciences* **7**(12), 164 (2017).

129 D. H. Smith, V. E. Johnson, and W. Stewart, "Chronic neuropathologies of single and repetitive TBI: Substrates of dementia?," *Nature Reviews Neurology* **9**, 211–221 (2013).

130 A. Bittar, N. Bhatt, T. F. Hasan, *et al.*, "Neurotoxic tau oligomers after single versus repetitive mild traumatic brain injury," *Brain Communications* **1**(1) (2019).

131 Y. Wang and T. Liu, "Quantitative susceptibility mapping (QSM): Decoding MRI data for a tissue magnetic biomarker," *Magnetic Resonance in Medicine* **73**(1), 82–101 (2015).

132 J. Lee, S. Ji, and S. H. Oh, "So You Want to Image Myelin Using MRI: Magnetic Susceptibility Source Separation for Myelin Imaging," *Magnetic resonance in medical sciences : MRMS : an official journal of Japan Society of Magnetic Resonance in Medicine* **23**(3), 291–306 (2024).

133 Z. Li, R. Feng, Q. Liu, *et al.*, "APART-QSM: An improved sub-voxel quantitative susceptibility mapping for susceptibility source separation using an iterative data fitting method," *NeuroImage* **274** (2023).

134 H. G. Shin, J. Lee, Y. H. Yun, *et al.*, "$\chi$-separation: Magnetic susceptibility source separation toward iron and myelin mapping in the brain," *NeuroImage* **240** (2021).

135 M. J. Bedggood, C. A. Essex, A. Theadom, *et al.*, "Individual-level analysis of MRI T2 relaxometry in mild traumatic brain injury: Possible indications of brain inflammation," *NeuroImage: Clinical* **43** (2024).

136 J. F. Domínguez, A. Stewart, A. Burmester, *et al.*, "Improving quantitative susceptibility mapping for the identification of traumatic brain injury neurodegeneration at the individual level," *Zeitschrift fur Medizinische Physik* (2024).

137 K. Wunderle, K. M. Hoeger, E. Wasserman, *et al.*, "Menstrual phase as predictor of outcome after mild traumatic brain injury in women," *Journal of Head Trauma Rehabilitation* **29**(5), E1–E8 (2014).

138 V. Gallagher, N. Kramer, K. Abbott, *et al.*, "The effects of sex differences and hormonal contraception on outcomes after collegiate sports-related concussion," *Journal of Neurotrauma* **35**(11), 1242–1247 (2018).

139 R. T. Tierney, M. R. Sitler, C. B. Swanik, *et al.*, "Gender differences in head-neck segmnet dynamic stabilization during head accelaration," *Medicine and Science in Sports and Exercise* **37**(2), 272–279 (2005).